

## ToF in heavy ion reaction: CHIMERA detector and ISODEC experiment

S. PIRRONE<sup>(1)</sup>, G. CARDELLA<sup>(1)</sup>, E. DE FILIPPO<sup>(1)</sup>, E. GERACI<sup>(1)(2)</sup>,  
B. GNOFFO<sup>(1)(3)</sup>, G. LANZALONE<sup>(4)(5)</sup>, N. S. MARTORANA<sup>(2)(5)</sup>, A. PAGANO<sup>(1)</sup>,  
E. V. PAGANO<sup>(5)</sup>, M. PAPA<sup>(1)</sup>, G. POLITI<sup>(1)(2)</sup>, F. RIZZO<sup>(2)(5)</sup>, P. RUSSOTTO<sup>(5)</sup>  
and M. TRIMARCHI<sup>(1)(6)</sup>

<sup>(1)</sup> INFN, Sezione di Catania - Catania, Italy

<sup>(2)</sup> Dipartimento di Fisica e Astronomia "Ettore Majorana", Università di Catania - Catania, Italy

<sup>(3)</sup> Centro Siciliano Fisica Nucleare e Struttura della Materia - Catania, Italy

<sup>(4)</sup> Università Kore - Enna, Italy

<sup>(5)</sup> INFN, Laboratori Nazionali del Sud - Catania, Italy

<sup>(6)</sup> Dipartimento di Scienze Matematiche e Informatiche, Scienze Fisiche e Scienze della Terra, Università di Messina - Messina, Italy

received 2 March 2020

**Summary.** — The CHIMERA detector is a powerful array to study heavy ions collisions in a large dynamical range from low to Fermi energy. A summary of its characteristics and the applied identification methods is reported. In particular, we highlight the relevance of the ToF technique in the reaction products identification process. Among the many experiments realized by using the CHIMERA detector since 2000, in this work we present the results of the ISODEC experiment, a recent study on the neutron-poor  $^{78}\text{Kr}+^{40}\text{Ca}$  and the neutron-rich  $^{86}\text{Kr}+^{48}\text{Ca}$  systems, at 10 A MeV. For these reactions, we analyzed the fusion-evaporation and fission-like processes, and their dependence on the isospin, that is expected to play a crucial role in the onset of these processes.

### 1. – Introduction

In the field of the heavy ion collisions, some of the most advanced current researches concern the study of the nucleus structure and of the reaction mechanisms as a function of the isospin, *i.e.*, of the ratio  $N/Z$  of the studied nuclei, both in stable and in exotic nuclear systems. These studies need a high resolution in measuring charge, mass, energy and position of the reaction products.



Fig. 1. – CHIMERA in the scattering chamber at INFN-LNS.

The CHIMERA (Charged Heavy Ion Mass and Energy Resolving Array) array [1], installed at INFN, Laboratori Nazionali del Sud, is a  $4\pi$  detector, in which the measurement of ToF is one of the principal characteristics.

The CHIMERA detector, fig. 1, has been operating for a long time and has proven its capabilities to provide accurate results in the Fermi energy regime ( $E = 10\text{--}100\text{ MeV/nucleon}$ ) characterized by final states with a large number of charged products that populate a broad energy range [2, 3].

It is important to point out that CHIMERA has been conceived and built to study nuclear reactions at intermediate energy, around the Fermi energy, in particular to investigate relevant items as the equation of state of nuclear matter, the multifragmentation process, and the symmetry energy at low nuclear density.

In 2008 the capability of CHIMERA was improved with the implementation of the Pulse Shape Discrimination (PSD) in silicon detectors [4, 5]. Thanks to this upgrading, the operative domain of the array has been expanded at lower energy ( $E \leq 10\text{ MeV/nucleon}$ ), extending the field of the dynamic studies from the multifragmentation to the fusion reactions.

## 2. – Chimera array

The device consists of 1192 detector telescopes, arranged on 9 rings in the forward part, covering a polar angle from  $1^\circ$  to  $30^\circ$ , and 17 rings in spherical configuration, covering from  $30^\circ$  to  $176^\circ$ .

The single detection telescope consists of a planar n-type silicon (Si) detector with thickness of about  $300\ \mu\text{m}$ , followed by a Caesium Iodide Thallium doped crystal, CsI(Tl), with thickness ranging from 12 cm at forward angles to 3 cm at backward angles, coupled to a photodiode.

Thanks to the structure and the compactness of the modules, the geometrical efficiency of CHIMERA is very high. In fact, by considering the entrance and the exit holes, the supports of each detector and of the target, the detectors of CHIMERA cover the 94% of the total solid angle.

The employed identification methods are:

- $E$ -ToF, for mass measurement, velocity and energy measurements of the detected particles;
- PSD (Pulse Shape Discrimination) in the Si detector, through rise-time evaluation of the energy signals, for charge particles stopped in the Si detector;
- $\Delta E$ - $E$ , for charge identification of particles punching through the Si detector and stopped in the CsI(Tl). This method allows also the isotopic discrimination for particles with atomic number  $Z < 10$ ;
- PSD (Pulse Shape Discrimination) in the CsI(Tl) detector, for isotopic identification of light charged particles stopped in CsI(Tl).

Notice that in CHIMERA the PSD of fragments is obtained mounting the Si detectors in direct mode in order to maintain the good timing performances needed for the ToF measurements.

Figure 2 shows an example of the energy *vs.* the rise time plot, obtained by the PSD methods in the Si detector, for the reaction  $^{64}\text{Ni}+^{124}\text{Sn}$  at 35 MeV/nucleon and at  $\theta_{lab} = 13.5^\circ$ . A good identification of the atomic number  $Z$ , up to  $Z = 20$  is obtained. The energy threshold for charge identification ranges from 4 to 8 MeV/nucleon, as a function of the increasing detected charge.

**2.1. Time of Flight technique.** – The direct measurement of the velocity through the ToF technique is one of the most peculiar characteristics which make the CHIMERA multidetector a unique tool in the study of heavy ion collisions. In addition, the combination of  $\Delta E$  and ToF measurements allows to evaluate the mass of the fragments stopped in the silicon detector.

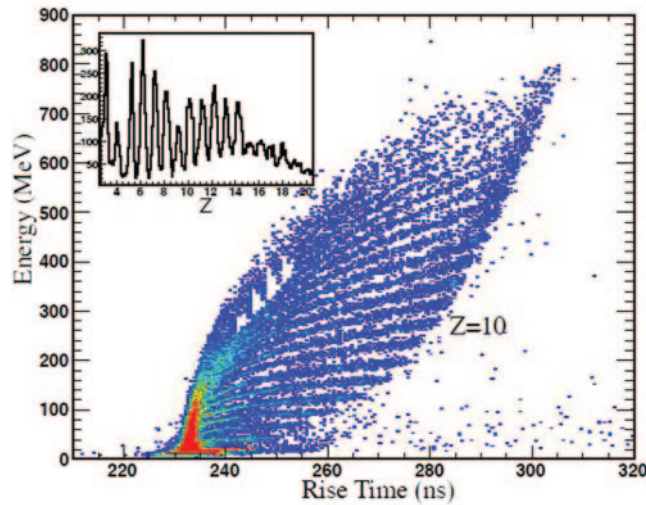


Fig. 2. – Energy *vs.* rise time for particles stopping in a silicon detector at around  $13.5^\circ$  for the reaction  $^{64}\text{Ni}+^{124}\text{Sn}$  at 35 AMeV. The inset shows the quality of the charge identification obtained in the experiment.

The Time of Flight measurement in CHIMERA is performed by measuring the difference in time between the delayed signal of the radio frequency of the cyclotron and the logic signal delivered by the CDF, acting on a given silicon detector, with a fraction set at 30% of the signal height. This difference is converted into channels  $t_{ch}$  by a TDC. The calibration line for each single detector is  $t(ns) = a(t_0 - t_{ch})$ .

It takes into account both the real Time of Flight and the delay due to cables, to the phase of the cyclotron and the delay in the formation of the signal in the silicon detector. All these effects are included in the time constant  $t_0$ , in channels units, depending on the specific detector and its electronics. This constant has to be accurately determined together with the conversion factor  $a$ , which is typically about 250 ps/channel.

We can observe:

- Particles, not having sufficient energy to punch through the silicon detector, lose all their energy and are stopped in this stage of the telescope. By using the ToF technique, they are identified in mass with the non-relativistic relationship, which relates energy to the Time of Flight:

$$E = \frac{1}{2} A \frac{d^2}{t^2},$$

where  $d$  is the distance of flight. The energy as a function of time results in  $1/t^2$  curves.

- Particles which punch through the silicon detector, having an energy loss  $\Delta E$  which linearly depends on  $Z^2$  and inversely on the velocity,

$$\Delta E \propto \frac{Z^2 t^2}{d^2} dx.$$

Plotting  $\Delta E$  as a function of time, it is possible to get curves that have a trend proportional to  $t^2$ . Figure 3 shows a bidimensional plot  $\Delta E$ -ToF, in which two zones A

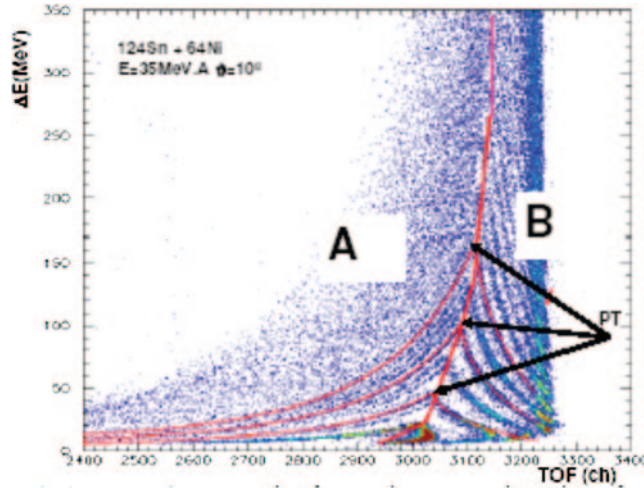


Fig. 3. –  $\Delta E$ -ToF matrix for a detector placed at  $\theta = 10^\circ$ , in the reaction  $^{124}\text{Sn} + ^{64}\text{Ni}$  at 35 A MeV.

and B can be distinguished. Zone A is occupied by particles which stop in silicon, while the curves of zone B are those related to particles punching through the silicon. The two zones are separated by the line passing through, corresponding to the silicon crossing areas.

A complex procedure, not reported here, was established to determine  $t_0$  and to find its possible dependence on energy and particle mass [6].

### 3. – ISODEC experiment

The first experiment realized by using CHIMERA in the low energy regime was the ISODEC experiment, in which we studied the isospin dependence of the decay of the  $^{118,134}\text{Ba}$  compound nuclei formed respectively in  $^{78}\text{Kr}+^{40}\text{Ca}$  and  $^{86}\text{Kr}+^{48}\text{Ca}$  reactions, at 10 AMeV [7-9].

The two investigated systems are different for 16 neutrons, the maximum difference that we can get by using stable nuclei; this allows to produce compound nuclei with both similar spin distribution and excitation energy in a large domain of  $N/Z$  (from 1.11 to 1.39).

In the experiment, self-supporting 1 mg/cm<sup>2</sup> thick  $^{40}\text{Ca}$  and  $^{48}\text{Ca}$  targets, prepared in collaboration between INFN-LNL and INFN-LNS Target Laboratories, were bombarded by  $^{78,86}\text{Kr}$  beams at 10 AMeV, delivered by the LNS Superconductive Cyclotron, with typical beam current intensity of 800–1000 pA. The pulsed beam was delivered with a timing resolution in the range 800 ps–1 ns. Inclusive and coincidence measurements were performed.

An example of isotopic identification is reported in fig. 4 for  $^{78}\text{Kr}+^{40}\text{Ca}$  and  $^{86}\text{Kr}+^{48}\text{Ca}$  at 10 MeV/nucleon. The mass distribution for carbon isotopes is obtained for all detectors at a polar angle of 15° [10].

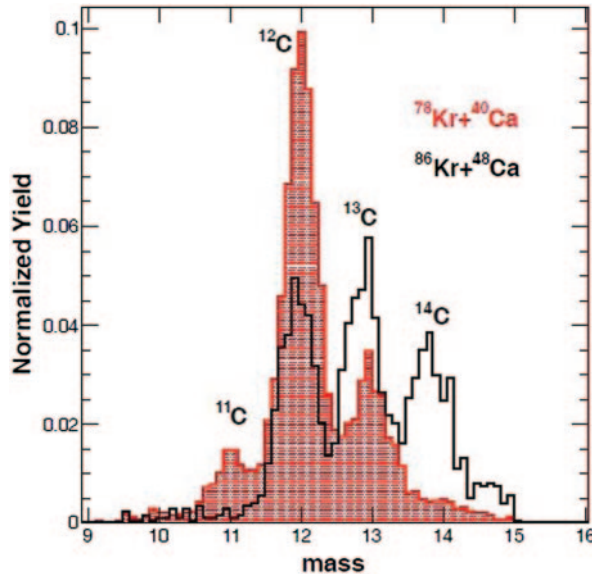


Fig. 4. – Mass distributions for charge  $Z = 6$ , for the two reactions  $^{78}\text{Kr}+^{40}\text{Ca}$  (red hatched histogram) and  $^{86}\text{Kr}+^{48}\text{Ca}$  at 10 AMeV.

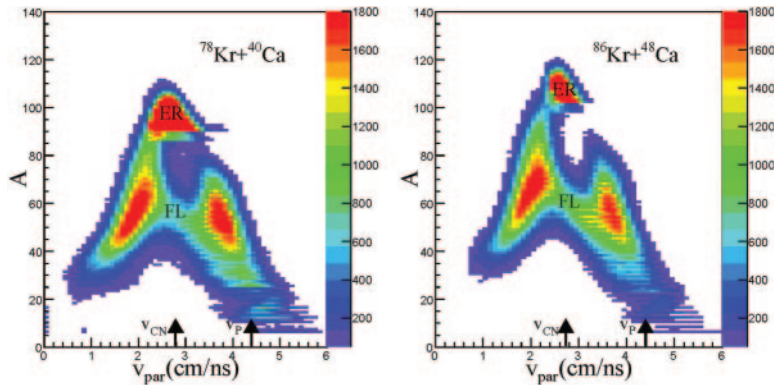


Fig. 5. – Mass *vs.* parallel velocity for reaction products detected in complete events for the two systems; the arrows indicate compound nucleus ( $v_{CN}$ ) and projectile velocity ( $v_P$ ) (the color scale of the Z-axis is in relative units).

All the aforementioned characteristics allowed the complete identification of light charge particle (LCP) in a wide energy range, the complete identification in charge and mass of fragments with  $Z = 3-10$ , punching through the Si detector, and the charge identification up to  $Z = 14-17$  for fragments stopped in the silicon. Mass was measured for all the detected fragments with different resolution ( $\Delta A = 1$  for  $A < 20$  and  $\Delta A < 4$  for  $20 < A < 100$ ). The charge of heavier fragments ( $Z > 18$ ) is then evaluated using EPAX code [11], as usually performed in the CHIMERA experiments.

Besides, we can apply the “complete event” selection, that means to select events in which we are able to detect at least 75% of the total mass and 60% of the total beam momentum involved in the reaction.

By applying the complete event selection, global decay patterns can also be studied through the plot in fig. 5, in which the mass  $A$  *vs.* the parallel velocity  $v_{par}$  is reported for each reaction product and for the two studied systems. In these plots we can distinguish the fragments coming from the different decay modes of the composite system formed in the reactions, as the Evaporation Residues (ER with  $90 \leq A \leq 110$  for the neutron-poor system and  $100 \leq A \leq 120$  for the neutron-rich one) centered around the compound nucleus velocity  $v_{CN}$  and the fission-like fragments (FL with  $10 \leq A \leq 85$  for the neutron-poor system and  $10 \leq A \leq 95$  for the neutron-rich one) distributed along the two branches, coming from the corresponding possible kinematic solutions.

These qualitative results concerning the isospin influence are confirmed quantitatively by the measurements of the cross sections for different processes presented in the following and obtained by the study of the angular distributions of the emitted fragments.

The study of the angular distributions of the emitted fragments provides fundamental information on their production mechanism. In fact, we can distinguish globally equilibrated processes, in which the compound nucleus formation is followed by evaporation or fission, from partially equilibrated processes as the fast-fission or the DIC processes.

Figure 6 reports some examples of angular distributions in the center of mass frame of fragments with various  $Z$ . The data are in good agreement with the  $1/\sin \theta_{cm}$  curve (full line), that is the shape expected for isotropic emission. This behavior is characteristic of production via a long-lived system, and implies a loss of the memory of the entrance channel direction.

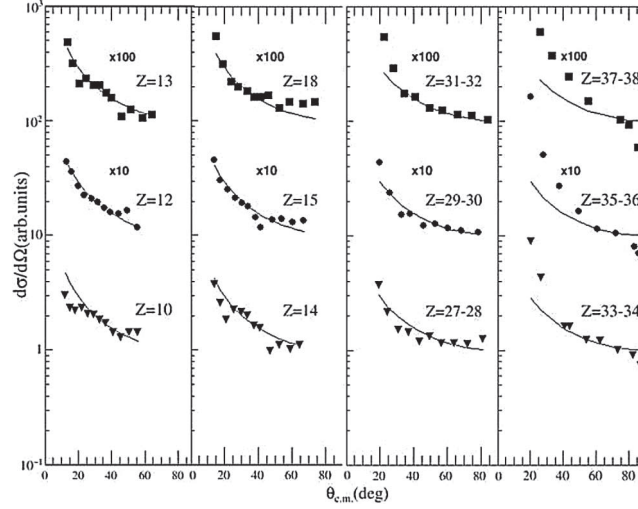


Fig. 6. – Angular distributions, in the center of mass frame, for some  $Z$  from 10 to 38 for the  $^{78}\text{Kr}+^{40}\text{Ca}$  reaction. The solid lines represent the function  $1/\sin\theta_{cm}$ .

However, we note that for  $Z > 30$  the experimental points have higher yields with respect to the  $1/\sin\theta_{cm}$  behavior, especially at small angles. This reveals the presence of an overlapping partially equilibrated mechanism involving a binary reaction process.

If we consider the angular distributions in the laboratory frame of some of the heavier reaction products ( $Z > 40$ ), as reported in fig. 7, we see that they are very strongly forward peaked, as expected in the case of evaporation residue, coming from both complete and incomplete fusion. Note that the contribution of fission-like process to the yield of very heavy fragments ( $Z = 41-44$ ) has been evaluated and subtracted from their

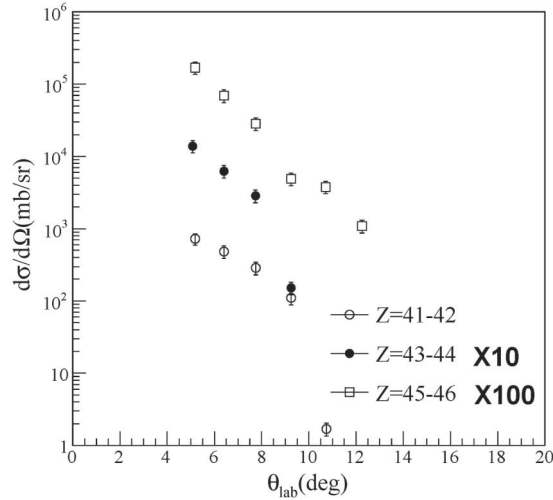


Fig. 7. – Heavy fragment angular distributions in the laboratory frame for the  $^{78}\text{Kr}+^{40}\text{Ca}$  reaction.

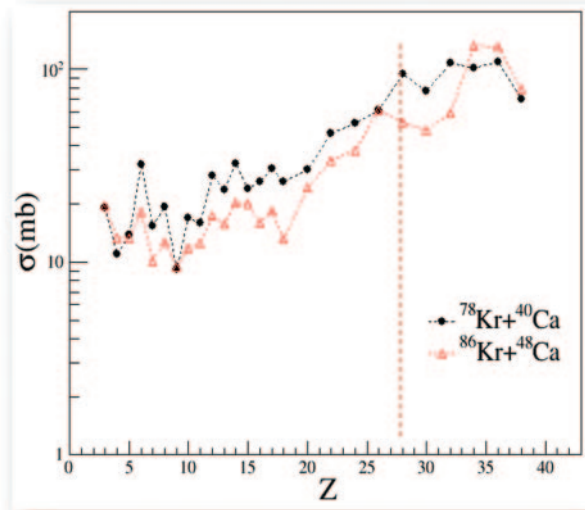


Fig. 8. – Charge distribution for the two systems.

production cross sections. The results of the angular distribution analysis presented here concern the neutron-poor system. Similar features and conclusions are obtained for the neutron-rich system.

By integrating the single angular distributions the production cross sections for each fragment are calculated and the resulting charge distribution is presented in fig. 8 up to  $Z = 38$ .

A strong even-odd staggering effect in the charge distributions is observed. This effect is due to a preferential production of fragments with an even value of the atomic number, because of the greater stability, afforded by larger binding energy [12]. In agreement with some other examples in the literature [13-15] the staggering is more pronounced for the neutron-poor system than the neutron-rich one, in particular for  $Z < 10$  reaction products. This effect persists for charges  $Z > 10$ , albeit with a smaller amplitude, but is not observed for  $Z > 17$ , where the cross sections are grouped two by two. We also observe that fragments production is globally favored in the  $^{78}\text{Kr}+^{40}\text{Ca}$  reaction, for which the cross sections are systematically higher.

The neutron enrichment seems thus to lower the cross sections of the lighter fragments, whose production can also be affected by structure effects, linked to the pairing forces [16]. As shown in fig. 8, the experimental charge distributions in both systems show an asymmetry around  $Z = 28$  (vertical dashed line), which would correspond to the symmetric fission of the composite systems. This asymmetry in the fragment yields could be due to a contamination from the DIC process mentioned in the previous section, producing heavier fragments at very forward angle, as observed in the angular distribution of fig. 6.

The measured production cross section for each fragment can provide an estimate of contributions of different decay modes of the composite systems in the two reactions. In particular, the cross section for evaporation residues can be obtained by considering all fragments with  $Z > 40$ , with the aforementioned subtraction of the contribution of heavier fragments from fission-like processes.

TABLE I. – *Evaporation residues, fission-like, fusion and total quarter point reaction cross sections for the two reactions.*

	$\sigma_{ER}$ (mb)	$\sigma_{FL}$ (mb)	$\sigma_{fus}$ (mb)	$l_{fus}$ ( $\hbar$ )	$\sigma_{reac}^{qp}$ (mb)
$^{78}\text{Kr}+^{40}\text{Ca}$	$455 \pm 70$	$850 \pm 120$	$1305 \pm 190$	117	$2390 \pm 250$
$^{86}\text{Kr}+^{48}\text{Ca}$	$400 \pm 60$	$530 \pm 85$	$930 \pm 145$	115	$2520 \pm 260$

The cross section for all fission-like mechanisms can be calculated by summing the contributions from  $Z = 3$  to the maximum yield in charge distributions, namely  $Z = 28/26$  for neutron-poor/neutron-rich system, respectively. This will ensure freedom from any contamination from DICs, whose contributions were discussed above.

The results are reported in table I, together with  $l_{fus}$  calculated from the  $\sigma_{fus}$  value, and with the values for reaction cross section  $\sigma_{reac}^{qp}$  calculated with the quarter point formula.

Estimated errors are a combination of the uncertainties in the integration procedure of the angular distributions and in the uncertainties in the calculation of the normalization constant. The fusion reaction cross sections ( $\sigma_{ER} + \sigma_{FL}$ ) are in agreement with a recent systematic study [17]. The difference between these values and the total reaction cross sections could be attributed to the already cited unequilibrated binary decay, which is more pronounced for the neutron-rich system.

#### 4. – Conclusions

The  $4\pi$  CHIMERA detector, operating since 2000 at INFN, Laboratori Nazionali del Sud, has been described. In particular, we emphasized the relevance of the Time of Flight measurement in the field of the heavy ion collisions.

Results of the study of the  $^{78}\text{Kr}+^{40}\text{Ca}$  and  $^{86}\text{Kr}+^{48}\text{Ca}$  reactions at 10 AMeV incident energy have been presented. Data have been taken with the CHIMERA device which operated for the first time in this lower energy regime, after the upgrade of the PSD in the silicon detector.

Indeed, in this experiment, because of the low energy, most of the reaction products are stopped in the silicon detector and their identification in charge and mass can be made mainly through the PSD in silicon and the ToF techniques.

Staggering effects are evident in the charge distributions of fragments with  $Z < 17$ , and are more pronounced for the neutron-poor system. A higher fragment yield is globally measured for the neutron-rich one. Some differences in charge distributions have also been observed with respect to the neutron-poor system studied at lower energy, suggesting different mechanisms and contributions to the reaction cross section as a function of energy. In particular evaporation is the favored decay mode at lower energy, while at higher energy the fusion fission channel prevails.

Cross sections of each element have been evaluated from the angular distributions. The single values of fragment production cross section have thus been used to reconstruct the total cross section of each reaction mechanism in both systems, in order to look for differences due to the  $N/Z$  degree of freedom. The results show that neutron enrichment seems to discourage the fusion process while inhibiting the fission decay process.

## REFERENCES

- [1] PAGANO A. *et al.*, *Nucl. Phys. A*, **734** (2004) 504.
- [2] DE FILIPPO E. and PAGANO A., *Eur. Phys. J. A*, **50** (2014) 32.
- [3] PEILERT G., STOCKER H. and GREINER W., *Rep. Prog. Phys.*, **57** (1994) 6.
- [4] POLITI G. *et al.*, *IEEE Nucl. Sci. Symp. Conf. Rec.*, **28** (2006) 1140.
- [5] ALDERIGHI M. *et al.*, *IEEE Trans. Nucl. Sci.*, **52** (2005) 1624.
- [6] GNOFFO B., PhD Thesis, University of Catania, Italy (2020).
- [7] PIRRONE S. *et al.*, *Eur. Phys. J. A*, **55** (2019) 22.
- [8] GNOFFO B., *Nuovo Cimento C*, **39** (2016) 275.
- [9] POLITI G. *et al.*, *JPS Conf. Proc.*, **6** (2015) 030082.
- [10] PIRRONE S. *et al.*, *AIP Conf. Proc.*, **1524** (2013) 7.
- [11] SUMMERER K. and BLANK B., *Phys. Rev. C*, **61** (2000) 034607.
- [12] GNOFFO B. *et al.*, *Eur. Phys. J. A*, **117** (2016) 08012.
- [13] LOMBARDO I. *et al.*, *Phys. Rev. C*, **84** (2011) 024613.
- [14] CASINI G. *et al.*, *Phys. Rev. C*, **86** (2012) 011602.
- [15] ADEMARD G. *et al.*, *Phys. Rev. C*, **83** (2011) 054619.
- [16] D'AGOSTINO M. *et al.*, *Nucl. Phys. A*, **861** (2011) 47.
- [17] EUDES P., BASRAK Z., SEBILLE F., DE LA MOTA V. and ROYER G., *Phys. Rev. C*, **90** (2014) 034609.